Mine Water and the Environment (2020) 39:57–67
https://doi.org/10.1007/s10230-020-00656-z

TECHNICAL ARTICLE

Study on the Height of the Mining-Induced Water-Conducting Fracture Zone Under the Q_{2l} Loess Cover of the Jurassic Coal Seam in Northern Shaanxi, China

Tingen Zhu[1] · Wenping Li[1] · Qiqing Wang[1] · Yanbo Hu[1] · Kaifang Fan[1] · Jiafa Du[1]

Received: 28 July 2019 / Accepted: 12 January 2020 / Published online: 20 January 2020
© Springer-Verlag GmbH Germany, part of Springer Nature 2020

Abstract
A method to calculate the height of a water-conducting fractured zone (HWCFZ) was developed based on the plate and shell theory, and the development of the HWCFZ in bedrock and Q_{2l} loess strata is discussed in detail. First, the subsidence-deflection curve equation of the overlying stratum is theoretically derived, and then the ultimate deflection and free space height of rock strata are calculated. Moreover, the strata tensile strain is calculated by using integral calculus. In addition, the failure state of the rock is analyzed by comparing the theoretically calculated tensile strain with the experimentally measured yield tensile strain, allowing one to attain the maximum value of HWCFZ. This approach was tested at the Jinjitan coal mine; the theoretically predicted, experimentally measured, and numerically computed maximum HWCFZ values were 189.5, 187.3, and 188.5 m, respectively, demonstrating the accuracy of the proposed method. These results are highly significant for safe and environment-friendly coal mining in northwest Shaanxi, China.

Keywords Plate and shell theory · Yield tensile strain · Field measurements · Numerical simulations

Introduction

Coal is China's major source of energy in China. In 2016, coal production and consumption supplied more than 70% of its energy (Liu et al. 2018; Zhang et al. 2009) and despite the continuous growth of renewable energy technologies, the total production and consumption of coal is expected to still exceed 50% of China's total energy resources in 2030 (Comprehensive Group on Consultation and Research in the Field of Energy 2015). The Jurassic coalfield in northern Shaanxi is China's largest coalfield, containing a third of China's total coal reserves (Yi 2008), and the coal seam is thick and shallowly buried. This means that large-scale and high-intensity mining is liable deform and destroy overlying strata, decreasing their capacity to supply water to the area. This has resulted in several issues, such as water inrush accidents in mines, industrial and agriculture problems, reduced vegetation, intensified desertification, and environmental concerns (Adam and Paul 2000; Andreas and Nikola 2011; Hu et al. 2019; Shao et al. 2014; Wang and Hang 2010).

Based on the deformation and failure characteristics of the overlying strata, there are three distinct zones of disturbance in overburden strata, i.e. the caved, fractured, and continuous deformation zones (Palchik 2003). The height of the water-conducting fractured zone (HWCFZ) is the sum of the heights of the fractured and caved zones (Adhikary and Guo 2014). Therefore, a method to accurately predict the maximum value of the HWCFZ is of great theoretical and practical significance.

Scholars have proposed different methods, including empirical formulas, statistical analysis, theoretical calculations, field measurements, and numerical simulations, to predict the maximum value of the HWCFZ. For instance, Liu (1995) carried out regression analysis of experimental data of different coal mines in north China and obtained an empirical formula. However, the geological conditions and mining technology are significantly different in the eastern and western parts of China. Therefore, the derived empirical formulas are not applicable to coal mines in northern

Electronic supplementary material The online version of this article (https://doi.org/10.1007/s10230-020-00656-z) contains supplementary material, which is available to authorized users.

✉ Wenping Li
wpligroup@cumt.edu.cn

[1] School of Resources and Geosciences, China University of Mining and Technology, Xuzhou, 221116 Jiangsu, China

Shaanxi (Fan and Zhang 2015). Hu et al. (2012) summarized the non-linear statistical relationship between the HWCFZ and the mining height, hard rock lithology ratio, coalface length, mining depth, and other mining factors, and obtained a formula to predict the HWCFZ based on different mining factors. Zhao and Wu (2018) predicted coal seam roof HWCFZ by random forest regression analysis. However, the selection of influencing factors, i.e. the determination of weight index and weight analysis, is based on the judgment of decision-makers, which can be influenced by several factors. Liu et al. (2015) analyzed the movement characteristics of overlying strata and e obtained a theoretical formula to predict the HWCFZ based on different mining factors. Majdi et al. (2012) considered the upper-pressure relief zone after coal seam mining and derived five mathematical methods to estimate the maximum value of the HWCFZ. Based on the failure characteristics of different lithologic rocks, Wang et al. (2012) established a computational mechanics model to predict the HWCFZ using the strain and stress as the indices of water flow in soft and hard rock strata. Che et al. (2016) proposed a novel approach to determine by constructing a damage range model of overlying strata, based on a theory of rock fragmentation and expansion and the basic principles of stress balance in underground space after mining. Zhang et al. (2017) applied system theory, and explained the process of overburden failure and generation of water-conducting fissure zone from an energy conservation viewpoint. This allowed the approximate value of the HWCFZ to be obtained by a system input–output method.

However, these theoretical methods are based on the development of the HWCFZ in bedrock, and does not consider the development of the HWCFZ in overburden soil. Sui et al. (2015) studied the changes in flushing fluid consumption, water level, drilling speed, air suction, and gas emission during drilling and used these to establish a rock quality designation (RQD) and systematically analyze the fracture development and the HWCFZ. However, in the case of large drillholes and well leakage, their method is unlikely to work. Lv et al. (2016) used borehole imaging to collect image information of borehole interiors and determined the development characteristics, connectivity and fragmentation of mining rock mass and obtained a HWCFZ value however, the proposed method can only be used in boreholes without water holes and casings. Zhang et al. (2018) targeted the recovery and exploitation of coal resources retained after fully mechanized top-coal caving mining, and used UDEC numerical simulation software and a multivariate non-linear regression analysis method to obtain a mathematical relationship for calculating the HWCFZ for block coal mining. And, based on the geological conditions and filling methods of a copper-lead–zinc mine and a coal mine, Liu et al. (2009) and Cheng et al. (2017) obtained HWCFZ values by fluid–solid coupling calculations in FLAC3D.

Q_{2l} loess is widely distributed in northwest China. It has a small elastic yield limit, obvious structural strength and collapsible deformation, and its mechanical properties are strongly affected by these characteristics. The development of the HWCFZ under the cover of the Q_{2l} loess is the root cause of typical water disasters in China's western mining area. Therefore, we developed an HWCFZ prediction method based on the plate and shell theory (Huang 1987) in theoretical analysis. The Jinjitan coal mine was used as a case study; the development of the HWCFZ was developed in overlying bedrock and the Q_{2l} loess was investigated using theoretical calculations, field measurements, and numerical simulations. The feasibility and accuracy of the theoretical calculation method was then verified by comparing the theoretically predicted results with field measurements and numerically computed results.

Study Region

The Jinjitan coal mine is located in Yulin city, Shaanxi province (Fig. 1a). The main landforms in the study area are wind-blown sand with scattered loess ridges and valley terrace landforms. The average annual rainfall in Yulin (2005–2015) can be estimated as 406.18 mm, and the rainfall in June, July, August and September accounts for about two-thirds of the total annual rainfall. Moreover, the average annual evaporation can be estimated as 1775 mm; thus, the region is arid-semiarid and its ecological environment is already fragile (Liu et al. 2019). The Quaternary phreatic aquifer mainly receives infiltration recharge from atmospheric precipitation, which is restricted by rainfall conditions, topography, and other factors. Given the high evaporation rate and coal mining, water resources are short and desertification is intensified. Therefore, the study area has become a key area for soil and water conservation and desertification control.

The strike and inclined length of the J coalface is 5.1 km and 300 m, respectively, and the mining area is 1.53 km^2 (Fig. 1b). The coal seam dip is sub-horizontal with a mining thickness of 8.6 to 11.2 m, at a depth of 259 to 284 m. The stratigraphic sequence of the study area is shown in Table 1.

Due to the shallow burial depth of the coal seam in the study area, the HWCFZ can penetrate through the bedrock into the Q_{2l} loess layer (Fig. 2). The Q_{2l} loess layer is the main relative aquifuge in the study area, and controls the leakage of phreatic water. The HWCFZ development decreases the waterproof performance and enhances water leakage of the phreatic aquifer in the sand layer of the Quaternary Salawusu formation.

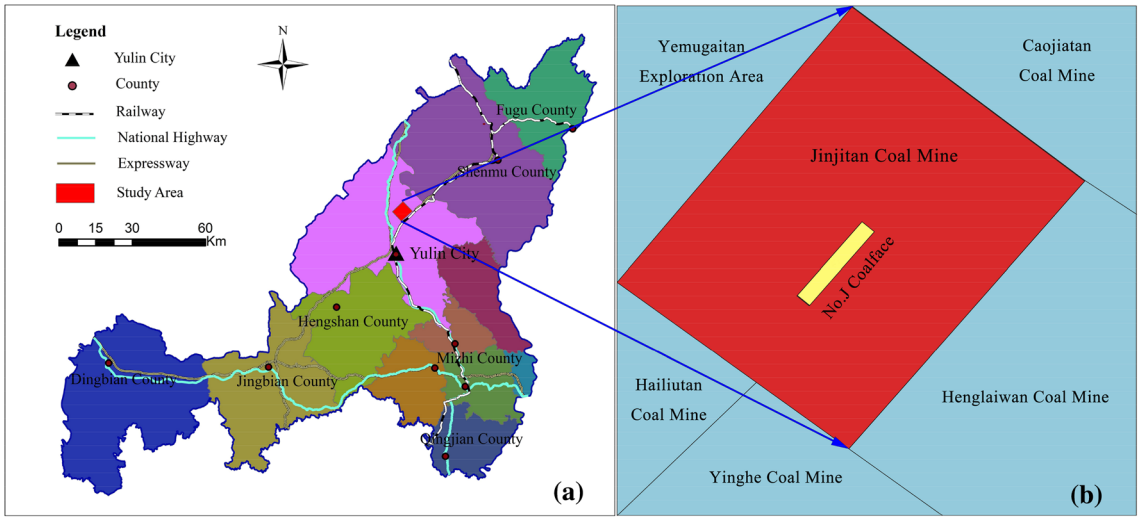

Fig. 1 Location of study area: **a** Jinjitan colliery in Yulin city, **b** No. J coalface of Jinjitan

Table 1 Stratigraphic information of the study area

Stratigraphic sequence	Stratum thickness (m) two pole value/average value	Stratigraphic characteristics
Q_4^{eol}	0–46.60/8.02	Widely distributed; the lithology is mainly yellow fine and silty sand
Q_{3s}	0–52.40/21.21	The lithology is mainly humus soil, silt, silty clay, and peat, as well as a gray-white medium grain, and a coarse grain sand layer
Q_{2l}	0–65.95/24.00	It is almost distributed in the whole area, and the lithology is yellow, brownish yellow clay and sandy soil
J_{2a}	0–47.04/25.66	It is distributed in the north of the study area, and the lithology is mainly feldspathic sandstone
J_{2z}	75.26–164.17/121.87	The lithology is mainly feldspathic quartz sandstone, feldspathic sandstone, siltstone, silty mudstone, and mudstone
J_{2y}		
Section 5	23.95–80.90/62.92	The lithology is mainly gray white medium and coarse-grained feldspar, with gray siltstone and mudstone in the upper part
Section 4	45.14–61.50/50.87	It contains no. 2 coal formation, and the middle and lower parts are mainly gray white fine-grained and medium-grained sandstone
Section 3	22.47–36.57/27.54	It contains no. 3 coal formation, mainly composed of siltstone and mudstone, with carbonaceous mudstone and a thin coal seam at the top
Section 2	66.02–85.33/73.69	It is distributed in the whole area, with little change in thickness. 4^{-4} and 4^{-3} coal seams are relatively thin
Section 1	69.23–97.99/77.36	Mudstone layer or siltstone is developed at the bottom, siltstone, medium-fine sandstone with a thick interbed of mudstone in the middle

Theoretical Analysis

Before mining, the surrounding rock is in a state of stress balance. However, the stress of the surrounding rock is redistributed by mining. Based on the redistributed stress, the overlying strata can be divided into decompression, pressurization, and pressure stabilization zones (Qian and Shi 2003). Herein, the strata in the decompression area above the coalface after mining was the research focus. According to the J coalface borehole data, the ratio of the thickness of overlying stratum to length (or width) of the coalface is far less than 1/5. Therefore, the overlying bedrock can be considered a thin plate with four fixed edges, and the fracture mechanism of the bedrock can be analyzed using the plate and shell theory (Hang et al. 1987). If the direction along the coalface is considered as the *x*-axis, a thin plate mechanical model of overlying bedrock strata,

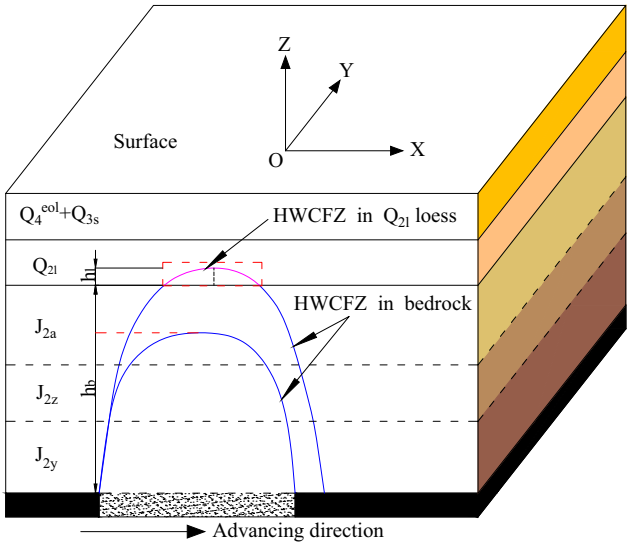

Fig. 2 HWCFZ in bedrock and Q_{2l} loess

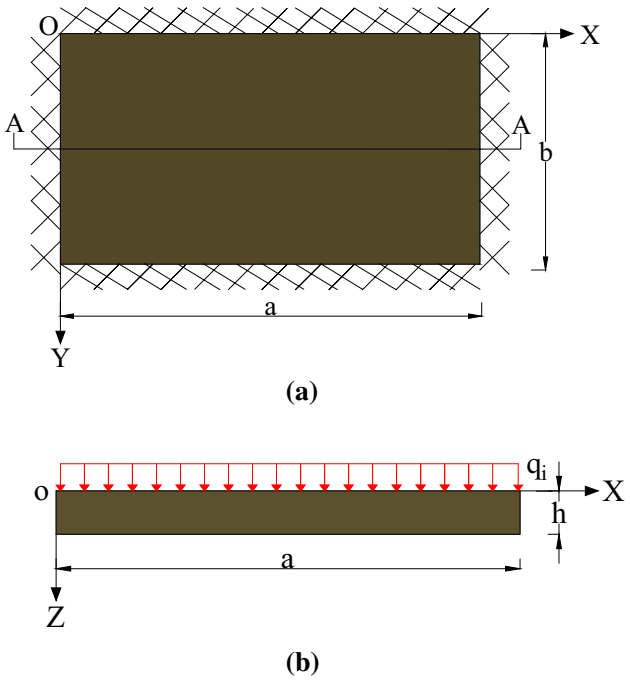

Fig. 3 Mechanical model of the stratum: **a** Top view, **b** A-A section

which is inclined to the *y*-axis and makes an intersection point at *o*, can be established, as shown in Fig. 3.

The equations and boundary conditions of the proposed mechanical model can be given as:

$$\frac{\partial^4 w}{\partial x^4} + 2\frac{\partial^4 w}{\partial x^2 \partial y^2} + \frac{\partial^4 w}{\partial y^4} = \frac{q(x,y)}{D} \tag{1}$$

$$(w)_{x=0} = (w)_{x=\mathrm{a}} = (w)_{y=a} = (w)_{y=b} = 0 \tag{2}$$

$$\left(\frac{\partial w}{\partial x}\right)_{x=0} = \left(\frac{\partial w}{\partial x}\right)_{x=\mathrm{a}} = \left(\frac{\partial w}{\partial y}\right)_{y=0} = \left(\frac{\partial w}{\partial y}\right)_{y=b} = 0 \tag{3}$$

where $q_{(x,y)}$ represents the load on each overlying bedrock and D refers to the flexural stiffness of the plate. The value of D can be given as: $\mathrm{D} = \frac{Eh_i^3}{12(1-\nu^2)}$. To satisfy the differential equation of elastic surface of the thin plate, the deflection function (w) can be represented as a triple series (Xu 2006).

$$\mathrm{w} = \sum_{m=1}^{\infty}\sum_{n=1}^{\infty} A_{mn} \sin\frac{m\pi x}{a} \sin\frac{n\pi y}{b} \tag{4}$$

where m and n represent positive integers (1, 2, 3…) and A_{mn} can be determined from Eq. (1). Therefore, $q_{(x,y)}$ can also be expanded into double trigonometric series at intervals [0, a] and [0, b], as given below:

$$q_{(x,y)} = \sum_{m=1}^{\infty}\sum_{n=1}^{\infty} a_{mn} \sin\frac{m\pi x}{a} \sin\frac{n\pi y}{b} \tag{5}$$

Herein, a_{mn} can be obtained from the orthogonality of the trigonometric function, $\sin\frac{m\pi x}{a}$ on [0, a]. Furthermore, by multiplying Eq. (5) by $\sin\frac{m\pi x}{a}$, $\sin\frac{n\pi y}{b}$ and integrating X and Y in [0, a] and [0, b] intervals, we can obtain a relationship for a_{mn}:

$$a_{mn} = \frac{4}{ab}\int_0^a\int_0^b q_{(x,y)} \sin\frac{m\pi x}{a} \sin\frac{n\pi y}{b} d_x d_y \tag{6}$$

By substituting Eq. (4) and Eq. (5) into Eq. (1), a simplified version of Eq. (6) can be obtained:

$$A_{mn} = \frac{a_{mn}}{\pi^4 D\left(\frac{m^2}{a^2} + \frac{n^2}{b^2}\right)^2} \tag{7}$$

Furthermore, by substituting A_{mn} into Eq. (4), a generalized solution of the deflection of four-sided clamped plates can be obtained:

$$\mathrm{w} = \frac{1}{\pi^4 D}\sum_{m=1}^{\infty}\sum_{n=1}^{\infty} \frac{a_{mn}}{\left(\frac{m^2}{a^2} + \frac{n^2}{b^2}\right)^2} \sin\frac{m\pi x}{a} \sin\frac{n\pi y}{b} \tag{8}$$

A mathematical expression for q_i can be obtained from the key stratum theory (Qian 2003) by assuming that the overlying bedrock in the coal seam is subjected to a uniformly distributed load (q_i), as given below:

$$q_i = \frac{E_i h_i^3 \left(\gamma_1 h_1 + \gamma_2 h_2 + \cdots + \gamma_n h_n\right)}{E_1 h_1^3 + E_2 h_2^3 + \cdots + E_n h_n^3} \tag{9}$$

Moreover, Eqs. (6, 7) can be used to obtain the deflection function of the overlying bedrock slab under a uniform load:

$$\mathrm{w} = \frac{16q_i}{\pi^6 D}\sum_{m=1}^{\infty}\sum_{n=1}^{\infty}\frac{1}{mn\left(\frac{m^2}{a^2}+\frac{n^2}{b^2}\right)^2}\sin\frac{m\pi x}{a}\sin\frac{n\pi y}{b} \tag{10}$$

One should note that the given series rapidly converges and only the 1st term needs to be satisfied (Huang 1987). Therefore, when $m=n=1$, the deflection function of the thin plate can be given as:

$$\mathrm{w} = \frac{16q_i}{\pi^6 D\left(\frac{1}{a^2}+\frac{1}{b^2}\right)^2}\sin\frac{\pi x}{a}\sin\frac{\pi y}{b} \tag{11}$$

However, at the central positions, i.e. $x = \frac{\mathrm{a}}{2}$ and $y = \frac{b}{2}$, of the thin plate, the deflection of the thin plate reached its maximum value: $w_{max} = \frac{16q_i}{\pi^6 D\left(\frac{1}{a^2}+\frac{1}{b^2}\right)^2}$.

The ultimate span a_m and b_m of the thin plate depends on the physical and mechanical properties, such as thickness and load of rock stratum. The failure condition of the thin plate can be given as: $\sigma_t > \left[\sigma_t\right]$. The a_m and b_m can be derived from the tensile strength of the plate (Liu et al. 2018):

$$a_m = \frac{ab_m}{b} \tag{12}$$

$$b_m = \sqrt{\frac{\sigma_t h^2}{6kq}} \tag{13}$$

Herein, K refers to the shape coefficient of the thin plate, as given below:

$$\mathrm{k} = 0.00302\left(\frac{a}{b}\right)^3 - 0.03567\left(\frac{a}{b}\right)^2 + 0.13953\left(\frac{a}{b}\right) - 0.05859 \tag{14}$$

Thus, the ultimate deflection function of bedrock thin plate in layer i can be given as:

$$w_{i-max} = \frac{16q_i}{\pi^6 D\left(\frac{1}{a_m^2}+\frac{1}{b_m^2}\right)^2}\sin\frac{\pi x}{a_m}\sin\frac{\pi y}{b_m} \tag{15}$$

HWCFZ Analysis

Compared with the horizontal state, the bent and subsided stratum is elongated after bending. Herein, the interlayer tensile deformation of strata is used to express this phenomenon. There is a direct relationship between the water conductivity and tensile deformation of strata (Gao et al. 2012). With the increase of strata elevation, the subsidence curve of the strata became gentler, and both the tensile deformation and fracture width of the strata gradually decreased. When the strata location reached a certain height, the generated micro-cracks were no longer conductive between the upper and lower layers due to the small amount of tensile deformation of rock strata. Hence, the development of water-conductive cracks is stopped, and the upper limit of the HWCFZ is attained.

In the process of overburden failure, only the strata within the range of the HWCFZ breaks up and produces fragmentation. The HWCFZ attained its maximum value when the coefficient of fragmentation of overburden collapse approaches the residual coefficient of fragmentation. The free space height below each caving stratum in the HWCFZ range (Qian 2003) can be given as:

$$\Delta_i = M - \sum_{j=1}^{i-1} h_i\left(k_j - 1\right) \tag{16}$$

where M refers to the mining thickness of coal seam and k_j represents the residual dilatancy coefficient of stratum j, which is taken as a reference (Liu 2018).

When $\mathrm{y} = b_m/2$, the arc length of the deflection curve of the clamped thin plate in [0, a_m] interval can be calculated from the curve integral method (Tongji University 2014)

$$S_{(x)} = 2\int_0^{\frac{a_m}{2}}\sqrt{1+w(x)'^2}d_x \tag{17}$$

Herein, the tension ratio of the bedrock layer can be given as:

$$\epsilon = \frac{S_{(0<x<a_m)} - a_m}{a_m} \tag{18}$$

The tensile strain (ε) of each bedrock stratum was calculated and compared with the yield tensile strain $\varepsilon_{[t]}$ of the corresponding bedrock. If $\Delta_i > w_{i-max}$ and $\epsilon > \varepsilon_{[t]}$ are tenable at the same time, the fissures between the bedrock conduct water and HWCFZ should continue to increase. On the other hand, if the HWCFZ steadily develops and does not continue to develop upward, this means that the HWCFZ develops to the maximum position. Hence, the maximum value of the HWCFZ can be given as: $H_{max} = h_b$ (Fig. 2).

When the coal seam is mined along the coalface to a certain length, the HWCFZ may penetrate the overlying bedrock and develop into the Q_{2l} loess layer. Herein, the Q_{2l} loess layer is considered as a weak rock layer, similar to the bedrock. Following the abovementioned steps, the free space height and actual tensile strain under the Q_{2l} loess layer are calculated, the top interface of the HWCFZ development in the Q_{2l} loess layer is analyzed, and the maximum value of HWCFZ is again given by: $H_{max} = h_b + h_L$ (Fig. 2).

Mechanical Theory Calculations

Determination of the Yield Tensile Strain of a Rock Stratum

In the current study, the direct uniaxial tensile tests of sandstone, sandy mudstone, mudstone, and Q_{21} loess were carried out using an MTS810 material testing machine and XL2101B5 strain tester (Fig. 4). Then, the experimental results were statistical analyzed to obtain the tensile strength and yield tensile strain of each stratum overlying the J coalface (Table 2). The experimentally measured yield tensile strain of the various rock strata revealed that the yield tensile strain of hard, medium-hard, soft, and weak strata were $\approx 0.05\%$, $\approx 0.10\%$, $\approx 0.20\%$, and $> 0.40\%$, respectively. These results are consistent with the previously reported yield tensile strain data of the strata (Gao et al. 2012).

Case Calculation and Analysis

Based on the drilling core data and indoor direct tension test, the overburden characteristics and physical and mechanical

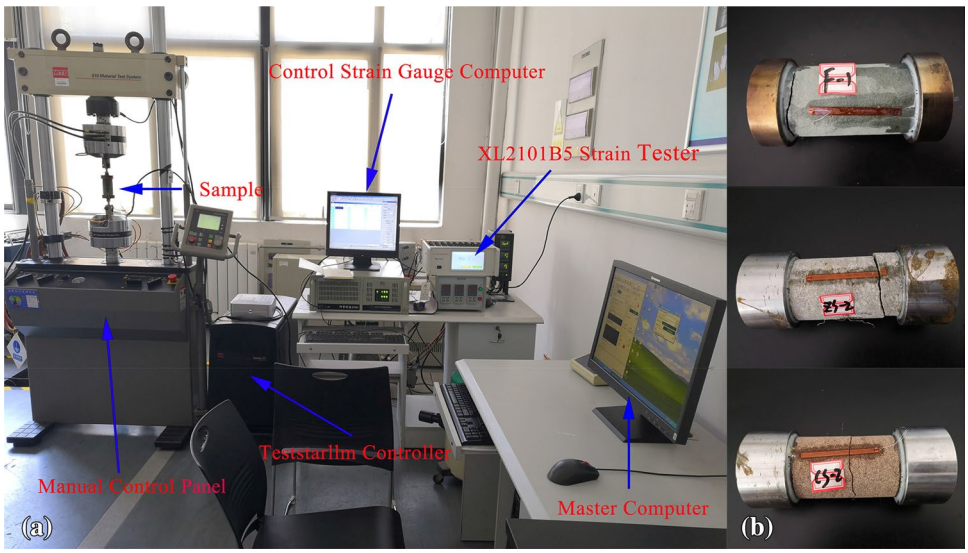

Fig. 4 Laboratory test: **a** MTS810 material testing machine and XL2101B5 strain tester; **b** sandstone after tensile failure

Table 2 Tensile strength and yield tensile strain of the strata overlying

Name	Number	Rm (Mpa)		Yield tensile strain (ε)	
		Measured value	Average value	Measured value	Average value
Q_2 loess	QL-1	0.05	0.05	0.00416	0.00405
	QL-2	0.05		0.00394	
Coarse-grained sandstone	CS-1	1.01	0.95	0.00050	0.00049
	CS-2	0.88		0.00048	
	CS-3	0.96		0.00048	
Medium grain sandstone	ZS-1	1.62	1.44	0.00059	0.00058
	ZS-2	1.25		0.00056	
	ZS-3	1.46		0.00057	
Fine sandstone	XS-1	2.65	2.55	0.00039	0.00038
	XS-2	2.59		0.00039	
	XS-3	2.42		0.00038	
Siltstone	FS-1	0.62	0.61	0.00099	0.00104
	FS-2	0.59		0.00101	
	FS-3	0.62		0.00111	
Sandy mudstone	SN-1	0.72	0.74	0.00191	0.00194
	SN-2	0.65		0.00191	
	SN-3	0.86		0.00201	
Mudstone	NY-1	1.13	1.05	0.00234	0.00159
	NY-2	0.96		0.00244	

parameters of the J coalface are given in supplemental table S-1. Taking the fourth layer as an example, the theoretical calculations are carried out according to the abovementioned method.

First, the height of the fourth layer stratum free space is calculated using Eq. (16):

$$S_4 = 8.6 - 11 \times (1.05 - 1) - 0.2 \times (1.035 - 1) - 0.25 \times (1.025 - 1) = 8.03 \text{ m}$$

Second, the maximum deflection of the fourth layer stratum is calculated using Eq. (11):

$$w_{4-\max} = 4 \times 10400.3 \times 2.045^4 \div \pi^6 \div 154.98 = 4.91 \text{ m}$$

Third, the actual tensile strength of the fourth layer stratum is calculated using Eq. (18):

$$\varepsilon_4 = (2.048 - 2.045) \div 20.45 = 0.0016$$

Finally, the maximum deflection, free space height, actual tensile strain, and yield tensile strain of the same layer were compared to determine whether the stratum was broken or not. Because $S_4 = 8.03 > w_{4-max} = 4.91$ and $\varepsilon_4 = 0.0016 > \varepsilon_{[4]} = 0.1\%$, the fourth layer stratum be regarded as broken. The failure state of each bedrock layer is obtained by the same calculation steps (supplemental table S-1).

To accurately determine the top interface of the HWCFZ during its passage through the overburden bedrock strata to the Q_{2l} loess, the 39.1 m thick Q_{2l} loess was subdivided into eight sublayers, with thicknesses of 3.6, 6.2, 3.8, 5.2, 4.6, 6.7, 5.4, and 3.6 m, based on the lithological description in the borehole column.

Following the above theoretical calculation steps, the free space height, maximum deflection and actual tensile strain of each layer were calculated. The results are compared and summarized in supplemental table S-1. Thus, the top interface of the HWCFZ in the Q_{2l} loess can be accurately determined. Based on these theoretical calculations, it can be concluded that the HWCFZ penetrates the overburden bedrock stratum and reaches the first small layer of the Q_{2l} loess, where it stabilizes and does not continue to develop further. Hence, the HWCFZ attained its maximum value, as given by: $H_{max} = h_b + h_L = 185.92 + 3.58 = 189.5$ m.

Field Measurements

Field monitoring of the dynamic deformation and failure of overlying strata was carried out using Brillouin optical time-domain reflectometry (BOTDR) distributed optical fiber sensing technology. The sensors were pushed into the monitoring hole before and after the mining of the J coalface, with a range of 400 m. The data were collected 1–2 times per day. The data were processed by an AV6419 Analyzer and Origin 2016 software. Figure 5 shows the strain distribution of the metal kieso sensing (MKS) optical cable in the JK2 borehole, where the *x*-axis represents strain and *y*-axis refers to the buried depth of the MKS (Liu 2018). Herein, the positive and negative strains indicate the tensile and compressive loads at the cable, respectively. The strain was measured after every 0.1 m. The curve shows that the peak value of tensile strain was + 12,200 με. However, after pushing through the borehole, the coalface was compressed again in the range of 77 to 200 m. When the overlying strata were relatively stable, the tensile strain and compressive strain of the cable were found to be + 1600 με and − 2750 με, respectively. With continuous advancement of the coalface, the overlying strata was gradually destroyed from the bottom to top.

To obtain the dynamic height of the overlying stratum, the deformation state of the overlying stratum was analyzed by comparing the strain of the optical fiber with the yield strain of the rock mechanics experiment. Figure 6 shows the distribution characteristics of deformation and failure zones of the overlying stratum when the distance of the panel and cable was – 52, 6, 46, 98, and 152 m. Under the influence of mining stress and deformation of the rock surrounding the roadway, the strata mainly renders tensile failure. Moreover, the area of tensile-strain-induced failure increased with the advancement of the coalface.

Based on the theoretical discussion and the position of the fiber optic tension–compression transition, it can be concluded that the rock under the HWCFZ experiences tensile load, whereas the rock above the HECFZ is mainly under compressive stress. Moreover, the experimental results of the MKS optical cable in JK2 borehole demonstrated that the buried depth of the maximum development position of the HWCFZ was 76.5 m, whereas the coal seam thickness was 11 m and the depth of the coal seam floor was 274.8 m.

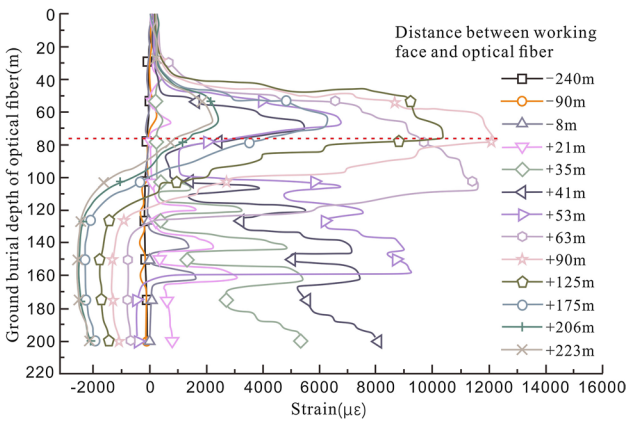

Fig. 5 The strain distribution of MKS cable

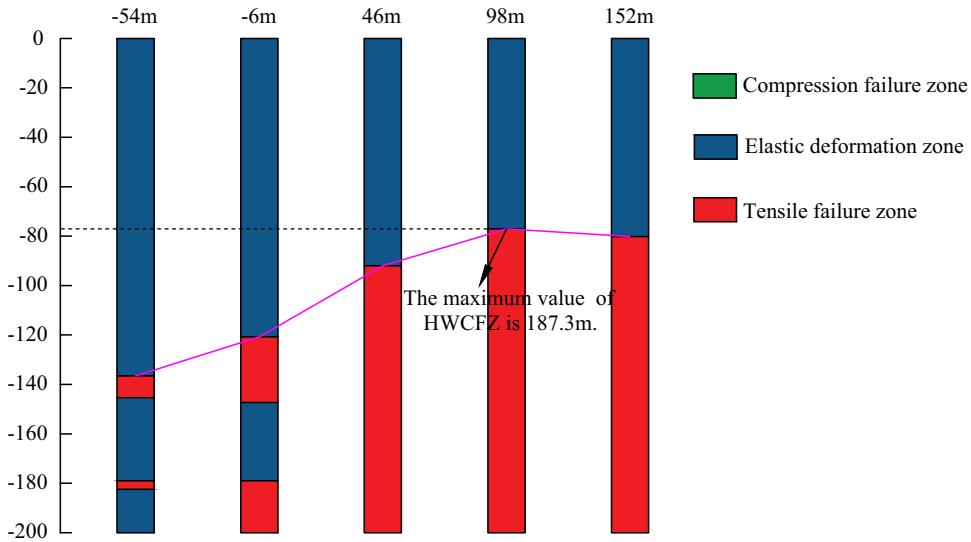

Fig. 6 Deformation and failure zoning of overburden

Therefore, the maximum value of the HWCFZ can be given as: $H_{max} = 274.8 - 76.5 - 11 = 187.3$ m.

To explore the change of permeability in the fractured rock mass caused by mining, a field water pressure test was carried out in the affected and unaffected areas in working face J using ground drilling. This method is generally used to evaluate the permeability of the rock and soil with poor permeability. In rock with good permeability (such as the rock in the fracture zone), the flow can suddenly increase several times and the pressure cannot be increased. Thus, the permeability of the main lithology (argillaceous sandstone, fine sandstone, and siltstone) in the upper, middle, and lower parts of the area not affected by mining was measured (see supplemental table S-2).

Numerical Simulations

Based on the physical and mechanical parameters of the overlying strata (supplemental table S-1), a soil-rock model was established according to the original roof strata and the development of the HWCFZ under the Q_{2l} loess. According to the mining plan of the coalface in the study area, the inclined length of the simulated mining face was 300 m and the planned simulated mining distance was 260 m. To eliminate the influence of boundary effects, 120 m protective coal pillars were placed on both sides of the model trend and 50 m protective coal pillars were placed on both sides of the model transverse. Thus, the model was set to be 500 m long and 400 m wide. To enhance stabilization of the proposed model, the Aeolian sand in the upper layer of the actual stratum was simplified to 0.4 MPa force, which acted on the top surface. The model height was 251 m. The boundary conditions were applied on four sides and the bottom of the model. The horizontal displacement in the lateral direction was fixed, whereas both vertical and horizontal displacements of the bottom boundary were fixed. The top of the model was allowed to move freely. The downward gravity stress and lateral gradient stress enhanced the consistency of the proposed model with actual mining conditions.

In general, the failure range of overburden is determined by distinguishing its plastic zone according to its strength and rock mechanics parameters. The range of the plastic zone gradually changes with the mining of coal seam and can be used as the overburden's failure zone (Tu and Yu 2004; Wang et al. 2005). The dynamic change in the plastic zone of the overlying stratum as the coalface advances is presented in Fig. 7. The failure characteristics of the overlying stratum is summarized below:

1. In the early stage of mining, tensile damage occurred above the goaf, and the height of the overburden failure remained low. The failure height of the overburden gradually increased as mining advanced. As the bearing limit of the rock beam above the goaf was not reached, the rock stratum does not collapse, the vertical displacement does not become obvious, and the rate of overburden failure remains slow. However, stress concentration occurred at both ends of the coalface and shear failure zones gradually appeared in the coal seam and surrounding rock in front of the opening eye of the coalface.
2. When the coalface advanced to ≈ 60 m, a small number of strata collapsed, shear failure occurred at both ends of the roof strata, and tensile failure occurred in the middle of strata. Furthermore, the rate of overburden failure obviously accelerated with continued mining. A few strata broke as the coalface advanced to ≈ 110 m.
3. As the coalface advanced to ≈ 140 m, tensile failure points gradually appeared in the strata. Moreover, the height of overburden failure gradually increased and the

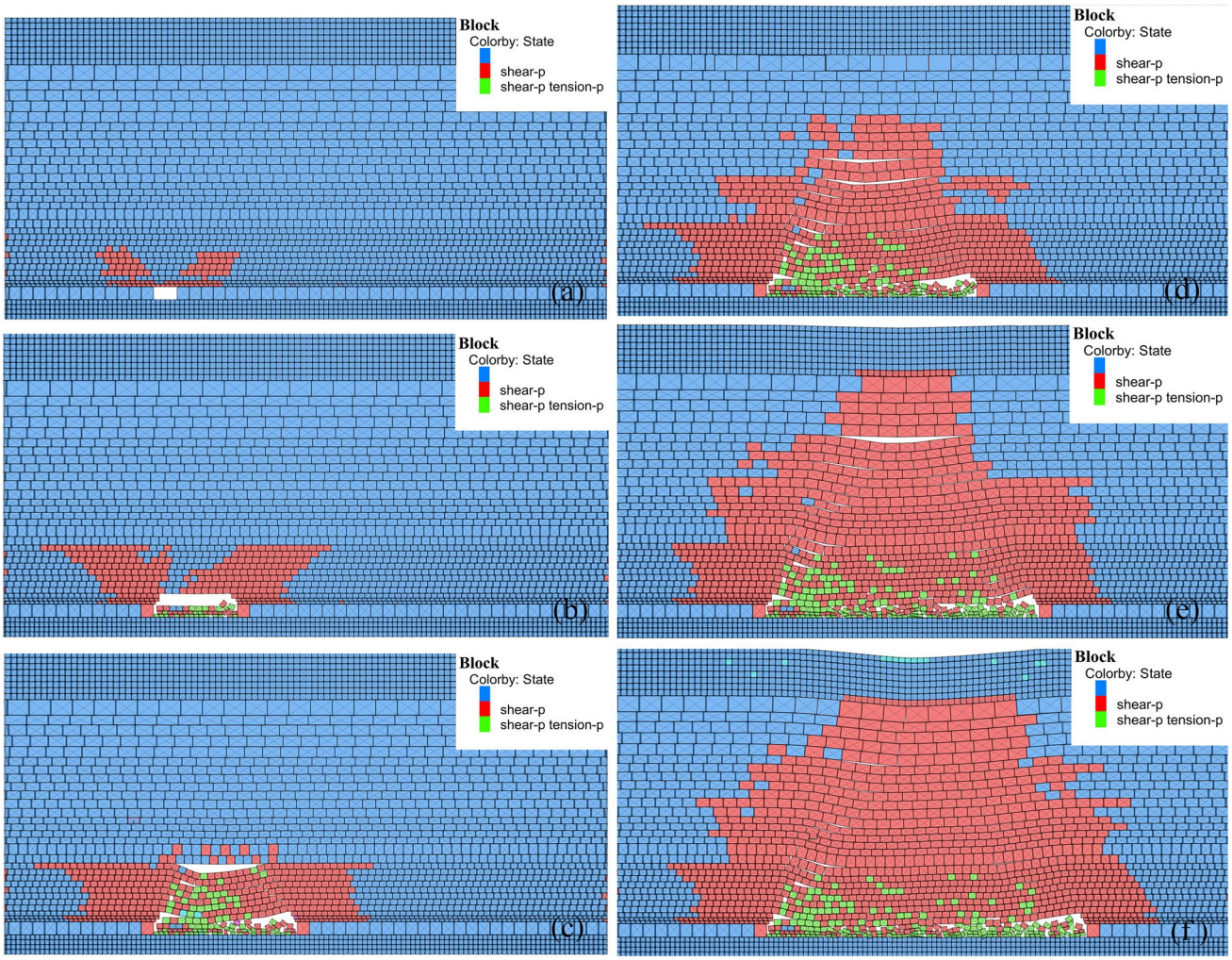

Fig. 7 The dynamic change of the plastic zone of the overlying strata in the model, propulsion distance of coalface: **a** 20 m, **b** 70 m, **c** 120 m, **d** 170 m, **e** 220 m, **f** 260 m

failure points become connected. When the coalface further advanced to ≈ 170 m, the rock beam and overburden rock were destroyed. As the coalface advanced from 140 to 210 m, the change in the plastic zone showed that overburden failure was not developing in a layer-by-layer scheme, as occurred initially, followed by a gradual increase and coalescence of local failure points.

4. When the coalface advanced to ≈ 220 m, the HWCFZ developed into the Q_{2l} loess and the bending and subsidence of the upper stratum compacted the cracks in the separated loess layer. As a result, the HWCFZ did not continue to develop upwards and remained stable or exhibited a relatively downward trend.

Based on the dynamic changes of the plastic zone, the HWCFZ-associated dynamics changes are presented in Fig. 8. The maximum value of HWCFZ was found to be 188.5 m.

Results and Discussion

The thick and shallow Jurassic coal seam in northern Shaanxi, China is prone to the formation and penetration of a HWCFZ through the overburden bedrock due to the large-scale and high-intensity mining, which can further develop into the Q_{2l} loess layer. As the empirical formulae of HWCFZ, summarized by Liu (1995), are not applicable to Northern Shaanxi (Fan and Zhang 2015), different reports on HWCFZ do not consider overlying soil (Che et al. 2016; Liu et al. 2015; Majdi et al. 2012; Wang et al. 2012; Zhao and Wu 2018). Therefore, a theoretical method was developed based on the plate and shell theory to predict HWCFZ values and the development of the HWCFZ in the bedrock and Q_{2l} loess. Field measurements and numerical simulations were carried out to demonstrate the accuracy and reliability of the proposed theoretical model.

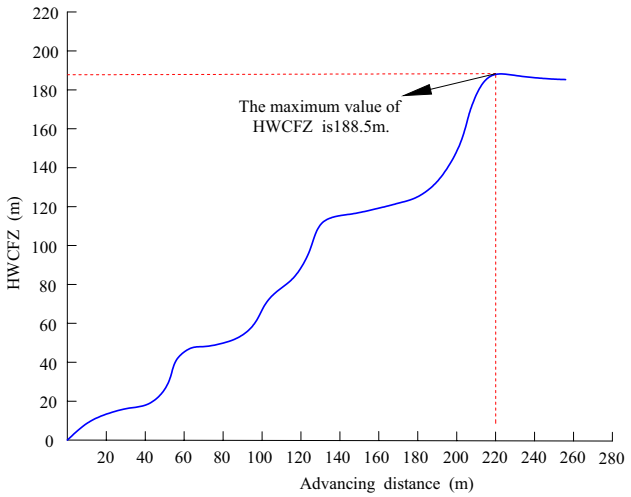

Fig. 8 The dynamic change of the HWCFZ in the model

One should note that the mechanical model of a thin plate, which was proposed by Tie et al. (1977), is based on the plate and shell theory. However, compared with the mechanical model of a masonry beam (Miao et al. 2011) and plastic hinge theory (Zhou et al. 2018), the mechanical model rendered comparable results to the actual situation of the overlying stratum. This was the first time that the mechanical thin plate model was used to analyze the development of the HWCFZ in a soil layer. Herein, $S_i > w_{i-max}$ and $\epsilon > \varepsilon_{[t]}$ were used simultaneously as a criterion of rock breakage. By using the J working face of the Jinjitan mine as a case study, the presented theoretical method predicted a maximum HWCFZ value of 189.5 ± 2.2 m.

Furthermore, field monitoring of dynamic deformation and failure of overlying strata based on BOTDR distributed optical fiber sensing technology, reveal that the experimentally measured maximum HWCFZ value was 187.3 m. One should note that optical fiber monitoring is a dynamic process. With the advancement of the borehole in the coalface, the stress recovery of the overlying stratum was slightly reduced. Hence, the experimentally measured HWCFZ value was slightly less than the theoretically predicted HWCFZ value. The numerical simulation results rendered a similar maximum HWCFZ value of 188.5 ± 1.2 m.

Conclusions

In summary, based on theoretical calculations, a novel calculation method was developed that accurately predicts HWCFZ values. The main research findings are summarized below:

1. The main steps of the calculation method are as follows: First, the subsidence-deflection curve equation of the overlying stratum was theoretically derived, and then, the ultimate deflection and free space height of the rock strata were calculated. Then, the strata tensile strain was calculated using integral calculus. Finally, the failure state was analyzed by comparing the theoretically calculated tensile strain with the experimentally measured yield tensile strain of each stratum, thus attaining the maximum HWCFZ value.
2. The theoretically predicted HWCFZ value was comparable to the experimentally measured and computed HWCFZ values, which demonstrated the reliability and accuracy of the proposed calculation method. These results are highly significant for safe, eco-friendly coal mining in the western mining areas of China, where conservation of groundwater resources is critical.
3. The proposed theoretical calculation method provides the basis for HWCFZ prediction, water hazard control and coal mining under water-containing in Jurassic coalfield of Northern Shaanxi, China.

Acknowledgements The study was jointly supported by the State Key Program of the National Natural Science Foundation of China (Grant 41430643) and the National Basic Research 973 Program of China (Grant 2015CB251601).

References

Adam PJ, Paul LY (2000) Broadening the scope of mine water environmental impact assessment: a UK perspective. Environ Impact Assess Rev 20:85–96

Adhikary DP, Guo H (2014) Measurement of longwall mining induced strata permeability. Geotech Geol Eng 32(3):617–626

Andreas K, Nikola R (2011) Sustainable development of energy, water and environment systems. Water Resour Manag 25:2917–2918

Che XY, Hou EK, Xie XS, Chen T, Feng J (2016) Analysis on development height of water flowing fractured zone in coal seam mining. China Sci Pap 11(3):270–273 **(in Chinese)**

Cheng L, Wang T, Qi P, Li YH (2017) Investigation of waterproof pillar design under aquifer in Cu-Pb-Zn mining of Xinzhuang. Eng J Wuhan Univ 50(3):368–374 **(in Chinese)**

Comprehensive Group on Consultation and Research in the Field of Energy (2015) Strategic research on clean, efficient, sustainable exploitation and utilization of coal in China. Strat Study CAE 17(9):001–005 **(in Chinese)**

Fan GW, Zhang DS (2015) Mechanisms of aquifer protection in underground coal mining. Mine Water Environ 34(1):95–104

Gao YF, Huang WP, Liu GL, Zhang SF, Zhu QM, Den ZY (2012) The relationship between permeable fractured zone and rock stratum tensile deformation. J Min Saf Eng 29(3):301–306 **(in Chinese)**

Hu XJ, Li WP, Cao DT, Liu MC (2012) Index of multiple factors and expected height of fully mechanized water flowing fractured zone. J China Coal Soc. 37(4):613–620 **(in Chinese)**

Hu YB, Li WP, Wang QQ, Liu SL, Wang ZK (2019) Evolution of floor water inrush from a structural fractured zone with confined water. Mine Water Environ 38(2):252–260

Huang KZ (1987) Theory of plates and shells. Tsinghua University Press, Beijing **(in Chinese)**

Liu TQ (1995) Influence of mining activities on mine rock mass and control engineering. J China Coal Soc 20(1):1–5 **(in Chinese)**

Liu Y (2018) Dynamic evolution and application of water conducting fractured zone during extraction of Jurassic coal seams in northern Shaanxi. Diss, China Univ of Mining and Technology

Liu B, He L, Luo L (2009) Numerical modeling on fluid-solid coupling for the waterproof coal pillar design. J Min Saf Eng 26(4):445-449,454 **(Chinese)**

Liu XS, Tan YL, Ning JG, Tian CL, Wang J (2015) The height of water-conducting fractured zones in longwall mining of shallow coal seams. Geotech Geol Eng 33(3):693–700

Liu SL, Li WP, Wang QQ (2018) Height of the water-flowing fractured zone of the Jurassic coal seam in northwestern China. Mine Water Environ 37:312–321

Liu Y, Liu QM, Li WP, Li T, He JH (2019) Height of water-conducting fractured zone in coal mining in the soil–rock composite structure overburdens. Environ Earth Sci 78(7):242

Lv GL, Yang L, Tian GJ, Zhang Y, Lv PT, Chen YB (2016) Detection and analysis of height of water flowing fractured zone in roof of fully mechanized caving face in deep and extra thick seam. China Coal 42(11):53–57 **(in Chinese)**

Majdi A, Hassani FP, Nasiri MY (2012) Prediction of the height of destressed zone above the mined panel roof in longwall coal mining. Int J Coal Geol 98:62–72

Miao XX, Cui XM, Wang JA, Xu JL (2011) The height of fractured water-conducting zone in undermined rock strata. Eng Geol 120:32–39

Palchik V (2003) Formation of fractured zones in overburden due to longwall mining. Environ Geol 44(1):28–38

Qian MG (2003) Key strata theory of strata control. China University of Mining and Technology Press, Xuzhou **(in Chinese)**

Qian MG, Shi PW (2003) Mine pressure and strata control. China University of Mining and Technology Press, Xuzhou **(in Chinese)**

Shao HQ, Wang JW, Xu SH, Gu SC (2014) The study of draining water drilling design method of Jurassic coalfield roof. Min Eng 12(6):59–61 **(in Chinese)**

Sui WH, Hang Y, Ma L, Wu Z, Zhou Y, Long G (2015) Interactions of overburden failure zones due to multiple-seam mining using longwall caving. Bull Eng Geol Environ 74(3):1019–1035

Tie MXK, Wo NSJ (1977) Theory of plates and shells. Science Press, Beijing **(in Chinese)**

Tongji University (2014) Advanced mathematics. Higher Education Press, Beijing **(in Chinese)**

Tu M, Yu ZL (2004) Analysis of overburden movement and failure in mining under extremely thick loose and strong aquifer. J Min Saf Eng 21(2):1–3 **(in Chinese)**

Wang SM, Hang QX (2010) Coal mining and ecological water level protection in ecologically fragile areas. Science Press, Beijing **(in Chinese)**

Wang SR, Wang JA, Dai Y (2005) Discrete element analysis of top coal movement and failure mechanism in fully mechanized caving mining in heavy inclined thick Seam. J Univ Sci Technol B 27(1):5–8 **(in Chinese)**

Wang LG, Wang ZS, Hang JH, Zhou DL (2012) Prediction on the height of water-flowing fractured zone for shallow seam covered with thin bedrock and thick windblown sands. J Min Saf Eng 29(5):607–612 **(in Chinese)**

Xu ZL (2006) Elastic mechanics. Higher Education Press, Beijing **(in Chinese)**

Yi MS (2008) Study and application of key strata theory in shallow seam of Shendong mining area. Diss, China Univ of Mining and Technology

Zhang DS, Fan GW, Ma LQ, Wang A, Liu YD (2009) Harmony of large-scale underground mining and surface ecological environment protection in desert district—a case study in Shendong mining area, northwest of China. Proc Earth Planet 1:1114–1120

Zhang JM, Zhang K, Cao ZG, Zhang Y (2017) Mining-bursting simulation and height calculation method for conducting-water fractured zone. J China Coal Soc 42(6):1557–1564 **(in Chinese)**

Zhang Y, Cao SG, Guo S, Wan T, Wang JJ (2018) Study on the height of fractured water-conducting zone under aquifer for short wall blocking mining. J Min Saf Eng 35(1):106–111 **(in Chinese)**

Zhao DK, Wu Q (2018) An approach to predict the height of fractured water-conducting zone of coal roof strata using random forest regression. Sci Rep 8:10986

Zhou Z, Zhao WS, Zhu CQ, Zhang KZ, Duan Y (2018) Prediction of water flowing fracture zone height based on the plastic hinge theory. Chin J Undergr Space Eng 14(5):1305–1312 **(in Chinese)**